

Equations of state of FeO and CaO

Raymond Jeanloz^{*} and Thomas J. Ahrens

*Seismological Laboratory, Division of Geological and Planetary Sciences, California
Institute of Technology, Pasadena, California 91125, USA*

Received 29 August 1979

Summary. New shock-wave (Hugoniot) and release-adiabatic data for $\text{Fe}_{0.94}\text{O}$ and CaO , to 230 and 175 GPa (2.3 and 1.75 Mbar) respectively, show that both oxides transform from their initial B1 (NaCl-type) structures at about 70 (± 10) GPa. CaO transforms to the B2 (CsCl-type) structure and FeO is inferred to do the same. Alternatively, FeO may undergo an electronic transition, but it probably does not disproportionate under shock to Fe and Fe_2O_3 or Fe_3O_4 . The Hugoniot data for the B1 phases of FeO and CaO agree with the ultrasonically-determined bulk moduli ($K_0 = 185, 112$ GPa, respectively) and with the ultrasonically-determined pressure derivative for CaO ($K'_0 = 4.8$); $K'_0 \sim 3.2$ for FeO is determined from the present data. The Hugoniot data for both FeO and CaO are consistent with low- and high-pressure phases having identical K_0 and K'_0 . Volume changes for B1/B2 transitions in oxides agree with theoretical expectations and with trends among the halides: $-\Delta V/V_1 \sim 4$ per cent and 11 per cent for FeO and CaO respectively. Also, the transition pressures increase with decreasing cation/anion radius ratio for the oxides. The Hugoniot data show that the density of the outer core is equal to that of a 50–50 mix (by weight) of Fe and FeO (~ 10 wt per cent oxygen), consistent with geochemical arguments for the presence of oxygen in the core. In terms of a mixture of simple oxides, the density of the lower mantle is satisfied by $\text{Fe}/(\text{Mg} + \text{Fe}) \sim 0.12$, however, arbitrarily large amounts of CaO can be present; an enrichment of refractory components in the lower mantle is allowed by the shock-wave data. Because of the relatively low transition pressure in FeO , a B1/B2 transition in $(\text{Mg}, \text{Fe})\text{O}$ is likely to occur in the lower mantle even if MgO transforms at 150–170 GPa. Such a transition may contribute to the scattering of seismic waves and change in velocity gradient found near the base of the mantle.

Introduction

FeO and CaO are the only major-element oxides which have not previously been studied at the high pressures existing in the Earth's mantle and core. We report the first Hugoniot

^{*} Present address: Department of Geological Sciences, Harvard University, Cambridge, Massachusetts 02138, USA.

(shock-wave), equation-of-state measurements for these oxides to pressure of 150 GPa (1.5 Mbar) and above. We believe that our results have special application to interpreting the state of the lower mantle and, in the case of FeO, that of the core.

The most important result of this work is the discovery of phase transitions in both oxides at about 70 GPa. Because of the density changes involved, these transitions allow considerable amounts of CaO and FeO to be present within the Earth. Similar transitions may occur in (Mg, Fe)O, which is thought to be prevalent throughout the lower mantle.

Although the phase assemblages which occur in the Earth's deep interior are unknown, it has long been recognized that the close-packed oxides have properties similar to those of the mantle (Birch 1952; Al'tshuler & Sharipdzhanov 1971). Hence, the simple oxides provide a model, high-pressure assemblage which is a convenient standard against which to reference other candidate phase assemblages. The present shock-wave data show that a wide range of oxide compositions can satisfy the properties of the lower mantle consistent, for example, with inhomogeneous accretion theories (Turekian & Clark 1969; Clark, Turekian & Grossman 1972). Some of the data for CaO which are presented below have been discussed by Jeanloz *et al.* (1979) who compare these with independent measurements made with the diamond-cell. They also compare the new data with the results of quantum mechanical calculations (Cohen & Gordon 1976), and find remarkable agreement between many of the predicted and observed properties of CaO at high pressures. In the following sections a description of the samples, an analysis of the shock-wave data, and their application to the mantle and core are discussed.

Samples and preparation

The iron oxide samples studied here are hot-pressed polycrystals from the same batch as studied by Graham & Bonczar (1978). Petrographic and microprobe analyses reveal the presence of 2.0 per cent (vol.) Fe, whereas a lattice parameter of $430.8 (\pm 0.4)$ pm was determined by X-ray diffraction. This indicates a stoichiometric coefficient $x = 0.94$ (in Fe_xO) according to Hentschel (1970), and hence a crystal density of $5.731 (\pm 0.004)$ Mg m^{-3} . A recent EXAFS study (Chen, Knapp & Chen 1978) demonstrates that no interstitial defects occur for $x \geq 0.90$, indicating that the present samples correspond structurally to stoichiometric wüstite (*cf.* Roth 1960; Kofstad 1972).

Archimedean densities were measured using reagent-grade Toluene and the correction factors of Berman (1939), but bulk densities were determined by directly measuring the volume of each sample (*cf.* Table 1). The porosity of the samples, derived from the bulk and crystal densities, is about 4 per cent and the near equivalence of bulk and Archimedean densities indicates that most of this porosity is not interconnected.

The CaO samples used in this study were all cut in {100} orientation (shock-wave propagation direction) from synthetic single crystals. These were grown by arc-fusion techniques and were acquired from two sources: (1) Oak Ridge National Laboratory (ORNL), samples grown and described by Abraham, Butler & Chen (1971); (2) CaO from the same batch (MRC) as used in the study of Son & Bartels (1972). X-ray diffraction and electron microprobe analyses produced no evidence of impurities. Because CaO is hygroscopic it was immersed in mineral oil for storage and cutting. Final sample preparation was carried out in a glove box under a controlled atmosphere and no evidence was found for even partial or superficial hydration of the samples used in this study.

The MRC samples are of variable colour ranging from clear to light brown (darker portions of the crystals were avoided), whereas the ORNL samples are uniformly clear; presumably the colour is due to carbon impurities (Freund, Debras & Demortier 1977;

Freund & Demortier 1978). Archimedean densities of virtually all of the CaO samples were found to be slightly less than the X-ray value $\rho_0 = 3.345 \text{ Mg m}^{-3}$ (Table 2). Infrared absorption spectra revealed a strong OH peak at 3645 cm^{-1} in several 1–2 mm thick chips from the ORNL crystals, indicating the presence of Ca(OH)_2 (portlandite) within these samples (e.g. Nakamoto 1970). Care was taken to prevent surface contamination or hydration, and the low values of density can be accounted for by the presence of up to 2.9 wt per cent portlandite within the CaO crystals. Briggs (1977) has similarly documented evidence for a brucite (Mg(OH)_2) precipitate within MgO grown by identical techniques as used for the CaO crystals.

Shock experiments and data analysis

Driver plates made of 2024 aluminium alloy, tantalum or tungsten were used, with fused quartz or Lexan arrival mirrors mounted on the back and on each side of the sample (e.g. Ahrens, Jackson & Jeanloz 1977). The driver plates are impacted by projectiles which are accelerated either by a two-stage light-gas gun or by a 40 mm propellant gun. The primary measurements consist of timing the projectile velocity and measuring the shock-wave travel time through the sample and mirrors (of known thickness) by way of a streak image such as is shown in Plate 1, and schematically in Fig. 1. Timing calibration marks are included directly on the streak image. Further experimental details are given in Jeanloz & Ahrens (1977, 1978), Ahrens *et al.* (1977) and Jackson & Ahrens (1979).

Impact velocities are measured with typical accuracies of about 0.1 per cent. The largest uncertainties in these experiments arise from reading the streak records which are interpreted from both a direct visual reading and also by means of microdensitometer scans (Jeanloz & Ahrens 1978; Jackson & Ahrens 1979). Between 25 and 50 scans are made across each streak record in a direction parallel to the time axis, and each of the boundaries corresponding to the shock wave entering or exiting the sample or mirrors is picked at the midpoint of the maximum gradient in light intensity (Plate 1). Time resolution is strictly limited by the graininess of the film at about 0.5–1.0 ns, however, the actual boundary locations are only determined to about 1.5 ns, or more, due to the fuzziness of the boundaries. This reflects, in part, the finite rise-time of the shock front.

A common difficulty arises from non-normal impacts as illustrated in Plate 1 and Fig. 1. The tilt of the projectile can reach up to $3\text{--}5^\circ$ at impact, however the particle velocity vector is still oriented normal to the driver plate and the boundaries on the streak record need only be fit by parallel lines which are not normal to the time axis. Ignoring for the moment projectile bowing (discussed below), the best fit to the boundaries corresponding

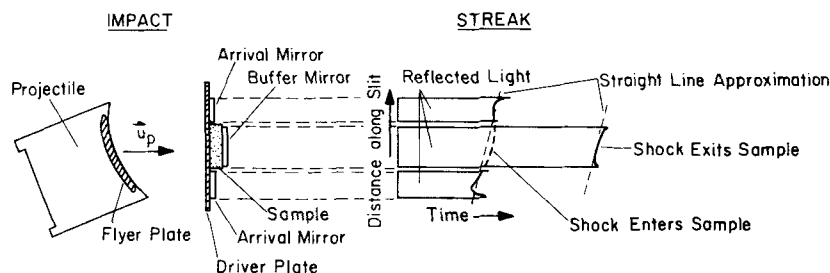


Figure 1. Schematic illustration (highly exaggerated) of projectile tilt and bowing, and their effect on the streak record. Particle-velocity vector (u_p) is normal to target (seen edge-on) despite tilt. The arrival on the streak record corresponding to the shock-wave entering the sample is significantly curved due to the bowing of the projectile.

to the shock entering the arrival mirrors (simultaneously, entering the sample), the buffer mirror (exiting the sample) and the buffer arrival mirror (exiting the buffer mirror) is given by the least-squares solution to a set of straight, parallel lines (e.g. Draper & Smith 1966). A weighting matrix can be determined by the sharpness of each boundary crossing, however, this is usually unnecessary. For convenience, the time axis is centred at the mid-point of the slit image. The least-squares analysis gives a direct estimate of the standard error of the intercept for each boundary, which is then used to evaluate the error in the determination of the shock-wave velocity.

A more difficult problem arises from bowing of the projectile, as schematically shown in Fig. 1. This commonly occurs at velocities above about 5.7 km s^{-1} (for Ta flyer plates) and produces a curved boundary on the streak record where the shock enters the sample. Corrections due to projectile bowing are large, up to about 15 ns (3–5 per cent of the travel time), although they only correspond to a 50–100 μm maximum flexure of the flyer plate. In reducing the data, a quadratic least-squares fit to the first boundary is found by an iterative scheme such that the slope at the centroid (intercept with the time axis) is parallel to the simultaneous least-squares fit to the remaining boundaries, which are taken to be parallel and straight. As is illustrated in Fig. 1, the straight line approximation is not good for the first boundary when the projectile is bowed, although it is a good approximation for the remaining boundaries (only one is shown) because these are relatively short and involve little extrapolation. The shortest travel time through the sample, which determines the shock-wave velocity, is given by the time interval measured along the centred time axis. Independent experiments in which the bowing is directly observed suggest that a quadratic fit and extrapolation of the first boundary, as used here, is adequate.

An important source of error results from non-uniform writing rate of the image-converter streak camera used for experiments with the light-gas gun (Plate 1). Although timing calibrations are performed for each experiment, the non-uniformity in writing rate can at times be determined only to 10 or 20 per cent. In reducing the data, a time-dependent writing rate is used which corresponds to the portion of the record being read.

Combining the errors just enumerated, the shock-wave velocity is usually determined to about 1 per cent (*cf.* Tables 1 and 2). A standard error analysis is used (e.g. Mood, Graybill & Boes 1974, p. 181), with most of the terms in the matrix of partial derivatives employed for the error propagation being given in Jackson & Ahrens (1979); additional terms have been included for uncertainties in initial density. The remaining data reduction employs the usual impedance matching conditions to determine Hugoniot states (e.g. Walsh & Christian 1955); the Riemann-integral equation is applied for release-path determinations (see Rice, McQueen & Walsh 1958; Lyzenga & Ahrens 1978; Jeanloz & Ahrens 1977, 1978). The standard equations of state of McQueen *et al.* (1970) for 2024 aluminium alloy, tantalum and tungsten, from Wackerle (1962) and Jackson & Ahrens (1979) for fused quartz, and from Carter & Marsh (1979) for Lexan were used in this study.

Results

The new shock-wave data for $\text{Fe}_{0.94}\text{O}$ and CaO are shown in Figs 2 and 3, and listed in Tables 1 and 2; both Hugoniot states and release adiabats are presented. For both compounds, there is clear evidence for a shock-induced phase transformation at approximately 70 GPa from the initial, B1 (NaCl-type) structure.

The properties of the B1 phases of both FeO and CaO have been studied extensively, in part because of the geophysical interest in these compounds (e.g. Mao *et al.* 1969; Akimoto 1972; Jackson, Liebermann & Ringwood 1978; Graham & Bonczar 1978; Son & Bartels

Table 1. Fe_{0.94}O shock-wave data.

Shot No.	EXPERIMENT		SAMPLE		HUGONIOT STATE			RELEASE STATE					
	Flyer/Driver	Impact Velocity (km/s)	Bulk Density (Mg/m ³)	Archimedeian Density (Mg/m ³)	Shock-wave Velocity (km/s)	Particle Velocity (km/s)	Pressure (GPa)	Density (Mg/m ³)	Buffer Material	Shock-wave Particle Velocity (km/s)	Pressure (GPa)	Density (Mg/m ³)	
457	W	1.705 ±0.001	5.499 ±0.004	5.525 ±0.008	6.435 ±0.050	1.220 ±0.003	43.2 ±0.2	6.785 ±0.016	Lexan	5.379 ±0.079	1.942 ±0.050	12.5 ±0.5	6.084 ±0.099
438	W	2.296 ±0.002	5.494 ±0.004	5.557 ±0.014	6.954 ±0.078	1.629 ±0.005	62.2 ±0.5	7.175 ±0.031	Lexan	6.117 ±0.115	2.412 ±0.073	17.7 ±0.9	6.530 ±0.124
471	W	2.500 ±0.003	5.504 ±0.007	5.522 ±0.010	7.173 ±0.045	1.766 ±0.004	69.7 ±0.3	7.301 ±0.020	Lexan	6.738 ±0.115	2.808 ±0.073	22.6 ±1.0	6.248 ±0.146
LGG 062	Al	5.101 ±0.004	5.484 ±0.005	5.563 ±0.014	7.221 ±0.042	2.034 ±0.007	80.6 ±0.2	7.635 ±0.027	Free surface velocity: fused quartz	3.165 ±0.329	5.922 3.034	39.6 ±1.7	6.058 ±0.485
LGG 046	Al	5.999 ±0.006	5.514 ±0.014	5.555 ±0.014	7.592 ±0.066	2.414 ±0.012	101.1 ±0.5	8.085 ±0.051	fused quartz	6.338 ±0.124	3.297 ±0.110	46.0 ±2.8	7.256 ±0.229
LGG 064	Cu	5.456 ±0.006	5.555 ±0.012	5.576 ±0.008	8.701 ±0.106	3.147 ±0.014	152.1 ±1.3	8.703 ±0.081	fused quartz	8.298 ±0.058	4.532 ±0.037	82.9 ±1.2	7.012 ±0.111
LGG 044	Ta	5.776 ±0.003	5.494 ±0.012	5.562 ±0.012	9.640 ±0.165	3.743 ±0.018	198.2 ±2.5	8.981 ±0.125	fused quartz	9.316 ±0.328	5.174 ±0.207	106.2 ±8.0	7.485 ±0.476
LGG 065	Ta	6.300 ±0.006	5.505 ±0.005	5.526 ±0.008	10.230 ±0.053	4.055 ±0.007	228.4 ±0.9	9.120 ±0.040	fused quartz	10.030 ±0.072	5.624 ±0.045	124.3 ±1.9	7.502 ±0.106

Note:

(1) Calculated from the shock-wave velocity measured through the buffer-mirror using:

$$\rho_0 = 2.204 \text{ Mg m}^{-3}, U_S = 1.11 + 1.59 u_p \text{ (km s}^{-1}\text{) (fused quartz)}.$$

$$\rho_0 = 1.196 \text{ Mg m}^{-3}, U_S = 2.33 + 1.57 u_p \text{ (km s}^{-1}\text{) (Lexan)}.$$

Table 2. CaO shock-wave data. Single crystals, {100} orientation.

EXPERIMENT	SAMPLE			HUGONIOT STATE					RELEASE STATE				
	Shot No.	Flyer/Driver	Impact Velocity (km/s)	Source (1)	Archimedeon Density (Mg/m ³)	Shock-wave Particle			Shock-wave Velocity (km/s)	Particle Velocity (km/s)	Pressure (GPa)	Density (Mg/m ³)	
						Velocity (km/s)	Velocity (km/s)	Pressure (GPa)					
428		W	2.342 ±0.060	B	3.306 ±0.001	8.204 ±0.101	1.801 ±0.048	48.9 ±1.4	4.236 ±0.036	5.202 ±0.210	2.581 ±0.132	29.6 ±2.7	3.737 ±0.237
												0	2.735
										Free surface velocity	±0.084		±0.081
LGG 060		A1	5.099 ±0.014	B	3.339 ±0.002	9.086 ±0.074	2.314 ±0.012	70.2 ±0.4	4.480 ±0.019	5.813 ±0.062	2.966 ±0.039	38.0 ±0.9	4.317 ±0.043
LGG 034		A1	5.226 ±0.020	B	3.305 ±0.003	8.312 ±0.166	2.491 ±0.020	68.4 ±0.7	4.719 ±0.050	No Data			(4) (5)
LGG 057		A1	5.992 ±0.004	0	3.325 ±0.002	8.831 ±0.063	2.846 ±0.009	83.6 ±0.6	4.906 ±0.024	6.116 ±0.122	3.409 ±0.077	49.0 ±2.0	4.695 ±0.072
LGG 027		Ta	4.510 ±0.020	0	3.345 ±0.004	9.068 ±0.100	3.285 ±0.011	99.6 ±0.9	5.245 ±0.041	7.334 ±0.150	3.924 ±0.095	63.4 ±2.8	4.952 ±0.111
LGG 040		Ta	5.197 ±0.004	B	3.307 ±0.006	9.630 ±0.048	3.782 ±0.005	120.5 ±0.5	5.446 ±0.022	8.223 ±0.034	4.800 ±0.21	92.3 ±0.8	4.537 ±0.054
LGG 024 (6)		Ta	5.680 ±0.110	0	3.319 ±0.002	9.706 ±0.097	4.151 ±0.087	133.7 ±3.0	5.798 ±0.104	7.422 ±0.148	3.980 ±0.093	65.1 ±2.8	5.784 ±0.093

LGG 055	Ta (thin)	5.608 ±0.005	0	3.347 ±0.002	10.253 ±0.082	4.038 ±0.008	138.6 ±0.9	5.521 ±0.035	9.270 ±0.110	5.145 ±0.069	105.1 ±2.7	4.593 ±0.159
LGG 052	Ta (thin)	5.817 ±0.006	0	3.338 ±0.002	10.579 ±0.087	4.174 ±0.009	147.4 ±1.0	5.513 ±0.036	9.467 ±0.098	5.269 ±0.062	109.9 ±2.4	4.686 ±0.127
LGG 033 (6)	Ta	6.075 ±0.006	0	3.312 ±0.005	10.159 ±0.102	4.421 ±0.010	148.7 ±1.2	5.864 ±0.054	7.960 ±0.160	4.319 ±0.101	75.8 ±3.3	5.859 ±0.054
LGG 049	Ta (thin)	6.101 0.006	B	3.315 ±0.002	10.577 ±0.110	4.402 ±0.011	154.3 ±1.3	5.678 ±0.052	9.869 ±0.150	5.523 ±0.095	120.1 ±3.9	4.697 ±0.230
LGG 043	Ta (thin)	6.219 ±0.004	B	3.320 ±0.002	10.877 ±0.188	4.465 ±0.018	161.3 ±2.2	5.630 ±0.084	9.200 ±0.321	5.101 ±0.202	103.4 ±7.7	5.417 ±0.177
LGG 047	Ta (thin)	6.473 ±0.004	B	3.328 ±0.002	11.233 ±0.170	4.628 ±0.016	173.0 ±2.0	5.659 ±0.215	10.149 ±0.073	5.699 ±0.139	127.5 ±5.9	4.951 ±0.245

Notes:

- (1) B: MRC samples; O: ORNL samples.
- (2) Calculated from the measured shock-wave velocity through the fused quartz buffer-mirror using: $\rho_0 = 2.204 \text{ Mg m}^{-3}$, $U_S = 1.11 + 1.59 u_p$ (km s^{-1}).
- (3) Based on first wave arrival: preferred interpretation.
- (4) Based on second wave arrival.
- (5) Poor record, results depend on interpretation.
- (6) Not shown in Fig. 4.

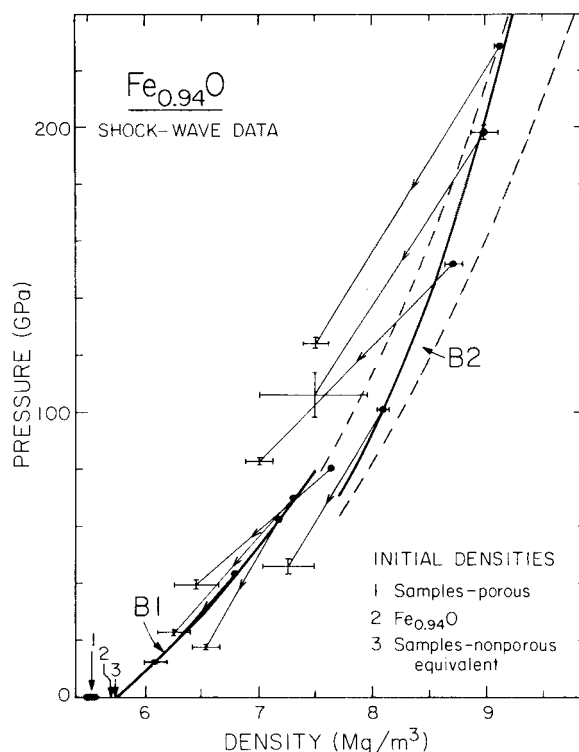


Figure 2. Hugoniot (solid points) and release-adiabat (error bars, no points) data for $\text{Fe}_{0.94}\text{O}$ (Table 1). The initial densities of the present samples, wüstite of the same stoichiometry and the non-porous equivalent (wüstite + iron) are shown. Dashed curves indicate envelope of theoretical Hugoniots calculated for the B2 phase (see Table 3). Free-surface result (shot 471) excluded for clarity.

1972; Sato, Ida & Akimoto 1973; Chang & Graham 1977). The present data are in good agreement with the results of most of these studies. For example, a least-squares fit (third order, Eulerian finite strain: see Jeanloz & Ahrens (1980) for details) to the CaO Hugoniot data determine the zero-pressure bulk modulus and its pressure derivatives, $K_{0S} = 111 \pm 3$ GPa and $K'_{0S} = 4.7 \pm 0.2$, in excellent agreement with the ultrasonically determined values of Chang & Graham (1977): 112.5 GPa and 4.8, respectively (*cf.* Jeanloz *et al.* 1979). These values are compatible with the results of previous static-compression (Perez-Albuerne & Drickamer 1965; Sato *et al.* 1973) and ultrasonic (Son & Bartels 1972) studies, however, the more recent work of Dragoo & Spain (1977) yields values that are significantly different. The best estimates of the properties of the B1 phases of FeO and CaO are listed in Table 3, which also provides the values of the Grüneisen parameters used in the present analysis.

In the case of Fe_xO , the present data are in excellent agreement with the value $K_{0S} = 185 \pm 5$ GPa measured ultrasonically by Jackson *et al.* (1978) and Graham & Bonczar (1978). This is illustrated in Fig. 4, in which the Hugoniot shown is based on the ultrasonic value of the bulk modulus, but with K'_0 unconstrained. With the K_{0S} thus constrained, the data require $K'_0 = 3.2 \pm 0.3$, whereas an unconstrained fit to the three shock-wave data results in $K_{0S} = 190 \pm 5$ (GPa), $K'_0 = 3.0 \pm 0.3$ (Table 3). The isotherm corresponding to the Hugoniot is also shown in Fig. 4, and it is evident that the earlier static-compression data (Clendenen & Drickamer 1966; Mao *et al.* 1969) are systematically offset from the calculated isotherm. We note that wüstite undergoes a magnetic transition at about 5 GPa (Vaughan & Drickamer 1967), which may affect the comparison of the static-compression and shock-wave measure-

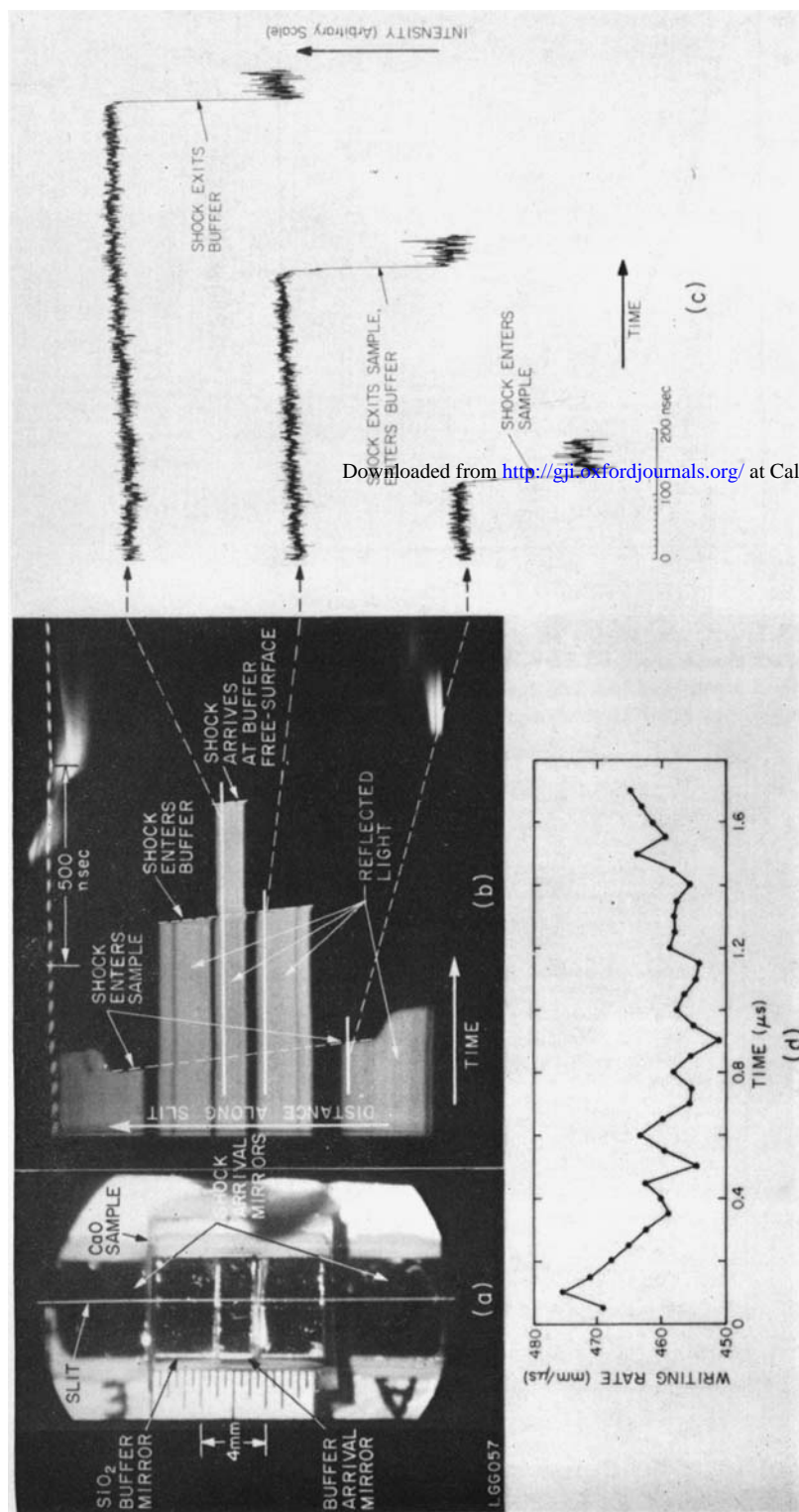


Plate 1. Experimental record for shot LGG 057 on CaO. (a) Still photograph of back side of target showing side arrival mirrors (A and E) and sample on driver plate. Buffer mirror and scale are placed on back of sample, and buffer arrival mirror is placed on back of buffer mirror. Position of slit is also indicated. (b) Streak photograph produced by sweeping the image, as viewed through the slit, of the back side of the target to the right. The successive destruction of shock-arrival, buffer and buffer-arrival mirrors by the shock wave is recorded by the disappearance of the light reflected from these mirrors. Time calibration shown at top. Note the tilt due to non-normal impact. (c) Microdensitometer records corresponding to the three traces shown on the streak record (not corrected for tilt). Shock arrival times are indicated. (d) Calibration of image-converter streak camera: writing rate is determined from microdensitometer scan of time calibration on streak record (stack of ten records shown).

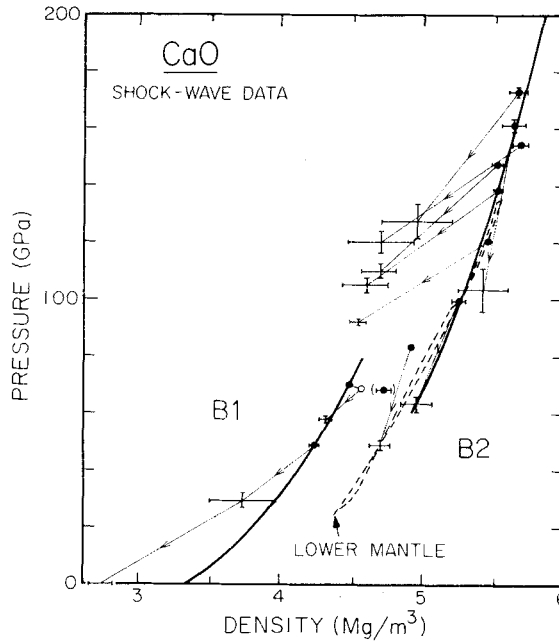


Figure 3. Hugoniot and release-adiabat data for CaO in B1 and B2 structures (Table 2); symbols are as in Fig. 2. Seismologically determined compression curves for the lower mantle are given as short-dashed lines. Open Hugoniot point shows the alternative interpretation of experiment LGG 060, and the datum in parentheses (LGG 034) is highly uncertain. Data from shots LGG 024 and 033 are not included (see text).

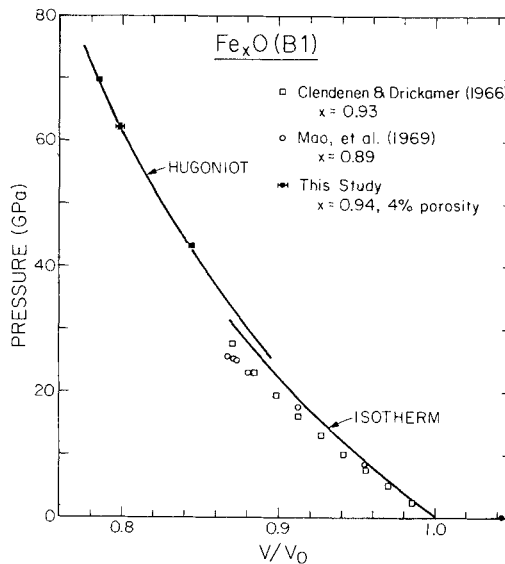


Figure 4. Compression data for wüstite in the B1 structure. The theoretical Hugoniot calculated from ultrasonic data (see text, K'_0 unconstrained) is shown, along with the corresponding isotherm. Isothermal static-compression and shock-wave data are given as open and closed symbols, respectively.

ments. Nevertheless, the new Hugoniot data support the ultrasonically measured value of K_0 rather than the value derived from static compression. The initial density (ρ_0) of FeO is not well determined (Table 3) because of the effect of non-stoichiometry on the lattice parameter of wüstite (e.g. Bénard 1954; Katsura *et al.* 1967; Hentschel 1970; Hayakawa, Cohen & Reed 1972).

Because many compounds with a B1 structure transform to the B2 (CsCl-type) structure at high pressures (e.g. Pistorius 1976), the transitions exhibited by FeO and CaO (Figs 2 and 3) might be expected to be of this type. Sluggish kinetics are not likely to seriously affect the shock data for a displacive transition, such as a B1/B2 type (Johnson & Mitchell 1972). Although {100}-oriented crystals, such as used here for CaO, may transform at slightly higher pressure than {111} crystals due to kinetics, this is likely to be a relatively small effect (see Fritz, *et al.* 1971; Duvall & Graham 1977). From *in-situ* X-ray diffraction at high pressures, the transition in CaO is known to be of B1/B2 type and it begins under shock within 10 GPa of the static transition pressure (Jeanloz *et al.* 1979). The present data can not conclusively determine the nature of the FeO transition, however, for both CaO and FeO the transition begins between 60 and 80 GPa under shock. Although the record for experiment LGG 060 on CaO can not be unambiguously interpreted, the preferred interpretation is that it documents a two-wave structure with the first (70 GPa) wave being associated with the B1/B2 transition. The alternative interpretation of that record is also given in Fig. 3 and Table 2, and would imply a transition pressure between 60 and 70 GPa for CaO. Similarly, experiment LGG 034 (datum in parentheses, Fig. 3) was only partially successful and its interpretation is uncertain.

Systematic relations suggest that B1 and B2 phases should have similar values of K_{0S} and K'_0 (e.g. Davies 1976), and this is consistent with the present data for CaO and FeO. The properties of the high-pressure phases of these oxides can be derived from the Hugoniot data of Figs 2 and 3, the results being listed in Table 3. The same approach has been used as discussed above: a third order finite-strain equation of state is found by a least-squares fit (Jeanloz & Ahrens 1980). High values of γ_0 have been assumed for the high-pressure phases based on the work of Ramakrishnan, Hardy & Kennedy (1979; see also Jeanloz 1979; Jeanloz & Ahrens 1980) who show that γ increases significantly on transforming from B1 to B2 phases. The transformation energies ($E_{tr} \sim P_{tr} \Delta V_{tr}$) have been determined by extrapolation of the high-pressure phase Hugoniots to the approximate transition pressures, using the least-squares fit shock velocity (U_S) versus particle velocity (u_p) relations given in Table 3. The CaO data from shots LGG 024 and 033 are considered separately, below.

Because the B2 structure is a likely candidate for the high-pressure phase of FeO, theoretical Hugoniots were constructed based on the predicted properties of this structure (e.g. Jeanloz & Ahrens 1977; Jeanloz *et al.* 1979). The envelope of the family of Hugoniots thus calculated from third-order finite-strain theory and for a plausible range of parameters is shown in Fig. 2. The high-pressure data fall within this envelope, consistent with the predicted occurrence of the B2 phase, however, they exhibit a curvature which is not seen in the calculated Hugoniots. Since the four highest pressure Hugoniot points define a straight U_S - u_p trend, it is not likely that a further transition occurs in the 100–230 GPa pressure range. This suggests that a higher than third-order finite-strain expansion is required, and the solid curve shows one possible fourth-order solution ($\rho_0 = 6.2 \text{ Mg m}^{-3}$, $K_{0S} = 192 \text{ GPa}$, $K'_0 = 3.55$, $\xi_2 = 1.5$, $\gamma_0 = 2$, $n = 1$, $E_{tr} = 31 \text{ kJ mol}^{-1}$), which corresponds to a (constrained) least-squares fit to the data. The datum at 152 GPa is not discrepant because it derives from a sample with a slightly lower initial porosity than the other samples: correcting for this effect shifts the point to the solid curve. This solution is consistent with the parameters listed in Table 3 and is used for the subsequent analysis of the high-pressure data of FeO.

Table 3. Properties of FeO and CaO.

B1 phase	FeO	CaO
ρ_0 (Mg m ⁻³)	5.864 ± 0.045 (1)	3.345 ± 0.003 (2)
K_{0S} (GPa):	185 ± 5 (3)	112 ± 1 (4)
dK_0/dP	3.2 ± 0.3 (5)	4.8 ± 0.1 (4)
γ_0 :	1.63 ± 0.25 (2, 6)	1.51 ± 0.11 (2, 6)
	$\gamma/V = \text{constant}$ (7)	
B2 phase		
ρ_0 (Mg m ⁻³)	6.05 ± 0.15 (8)	3.76 ± 0.05 (8, 9)
K_{0S} (GPa):	195 ± 10 (8)	115 ± 8 (8)
dK_0/dP :	3.4 ± 5 (8)	4.9 ± 0.8 (8)
E_{tr} (kJ mol ⁻¹):	29 ± 3 (8)	90 ± 5 (8, 9)
γ_0 :	1.8 ± 0.2 (7, 10)	1.8 ± 0.2 (7, 10)
$n = d \ln \gamma / d \ln V$	1 to 1.5 (7)	1 to 1.5 (8)
	$U_S = 3.72$ + 1.59 u_p (km s ⁻¹) (8)	$U_S = 3.80$ + 1.59 (km s ⁻¹) (8, 11)

Notes and references

Zero subscript indicates evaluated at zero pressure. Values for FeO are corrected for non-stoichiometry where necessary.

- (1) Hentschel (1970).
- (2) Robie, Hemingway & Fisher (1978).
- (3) Jackson *et al.* (1978); Graham & Bonczar (1978); this study.
- (4) Chang & Graham (1977); this study.
- (5) From shock-wave data, with K_{0S} constrained within stated range.
- (6) Touloukian *et al.* (1977); data in table.
- (7) Assumed.
- (8) This study, from fits to Hugoniot data. The high-pressure phase of FeO may not be of B2 type: see text.
- (9) Jeanloz *et al.* (1979).
- (10) See Ramakrishnan *et al.* (1979).
- (11) Data from experiments LGG 024 and 033 excluded.

Whether these data correspond to the B2 structure or not does not strongly affect this analysis.

Once the properties of the high-pressure phases have been determined by a fit to the Hugoniot data, temperatures along the Hugoniot can be directly calculated (*cf.* Jeanloz & Ahrens 1980, and references therein). The results for CaO and FeO are given in Fig. 5, along with recent estimates of the geotherm in the lower mantle and core, for comparison. A Debye–Grüneisen model is used for calculating the specific heat, and anharmonic contributions of higher order are neglected. CaO is in the high-temperature regime above about 80 GPa and 1000 K on the Hugoniot, whereas FeO enters the high-temperature range at 300–400 K and low pressure. The main reason for the steeper rise in temperature along the Hugoniot of CaO as compared with that of FeO is due to the significantly higher density of the latter. Nevertheless, for both compounds a direct comparison of the Hugoniot with the measured properties of the earth can be made approximately within the pressure range 100–140 GPa.

For CaO and FeO, the agreement between the expected properties of the B2 phase and the observed properties of the shock-produced, high-pressure phase is rather good. Both from considerations of a simple ionic model for B1/B2 transitions (e.g. Pauling 1960; Wells

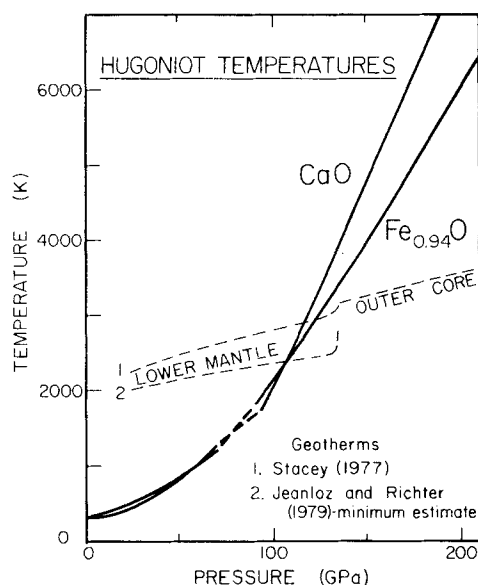


Figure 5. Calculated temperatures along the Hugoniot of CaO and $\text{Fe}_{0.94}\text{O}$; dashed portions indicate regions of phase transformation. Recently estimated geotherms for the lower mantle and outer core are also shown.

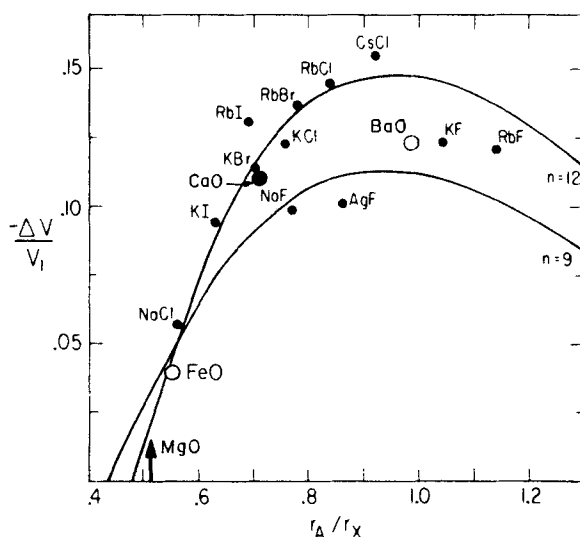


Figure 6. Correlation of relative volume decrease at the B1/B2 transition with ratio of cation/anion radii, from data and an ionic bonding model (solid lines; after Demarest *et al.* 1978). Two cases for repulsive potentials with r^{-9} and r^{-12} dependencies are given, and the ionic radii of Shannon (1976) were used. The nature of the FeO transition is uncertain and the case of BaO is complex (open symbols: see text). The radius ratio for MgO is also indicated.

1975) and from experimental data (e.g. Demarest, Cassell & Jamieson 1978), the volume change at the transition is expected to be determined by the ratio of ionic radii of the compound in question. As is illustrated in Fig. 6, such systematics are remarkably good for both halides and oxides (BaO involves complications due to the occurrence of distorted structures: Liu 1971; Liu & Bassett 1972). Similarly, the transition pressure from B1 to B2

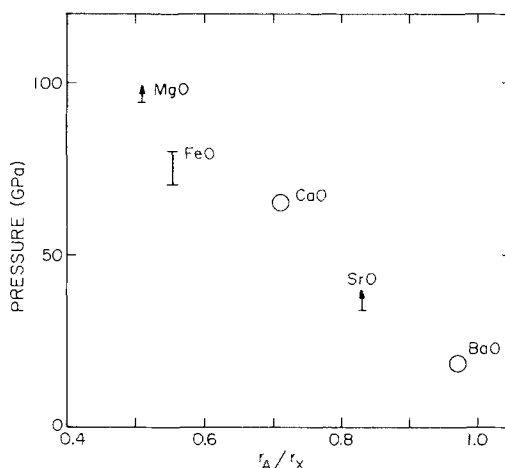


Figure 7. Correlation of transition pressures in B1 monoxides with radius ratio (see Fig. 6).

structures is expected to increase with decreasing cation/anion radii, at least qualitatively. Fig. 7 shows this to be the case for the data currently available for oxides. Both SrO and MgO are known to remain in the B1 phase (or distorted equivalent) to pressures of 34 and 95 (to 120) GPa, respectively (Liu & Bassett 1973; Mao & Bell 1979; Carter *et al.* 1971), hence only lower bounds can be given for the transition pressures of these compounds. The only other oxide for which a B1/B2 transition is known, EuO at 40 GPa, can not be directly compared in this respect since it is known to undergo a valence transition at about 30 GPa (Jayaraman 1972; Jayaraman *et al.* 1974). It is interesting to note that EuO does fit on the trend of Fig. 7 if the ionic radii for valence 2 are nevertheless used.

The high-pressure data for FeO can not be discussed further without considering what phase they may reflect. Several alternatives are listed in Table 4, and these can be distinguished as either structural or electronic transitions; a combination may also obtain. The occurrence of a distorted structure or of an unknown structure-type can not be ruled out, but these would likely have densities similar to or less than that of the B2 phase (as in BaO); FeO would be expected to further transform to a B2 structure. Disproportionation reactions of the type discussed by Mao (1974), Mao & Bell (1977), and Ringwood (1978) do not satisfy the present data, however. As is shown in Fig. 8, combinations of Fe₂O₃, Fe₃O₄ and Fe result in densities systematically less than those of FeO at high pressures (by

Table 4. FeO phase transition.

Structural	Predicted behaviour
(a) B1 (NaCl) → B2 (CsCl)	– $\Delta V/V \sim 4$ per cent, $P_{tr} \sim 90$ GPa
(b) Distorted structures	? – $\Delta V/V \leq 4$ per cent
(c) Disproportionation	– $\Delta V/V \leq 1$ per cent
Electronic	
(a) High spin → low spin	– $\Delta V/V \sim 20$ per cent, $K_0 \sim 250$ GPa, $P_{tr} \sim 25-40$ GPa – $\Delta V/V \sim 5$ per cent, $P_{tr} \sim 60-70$ GPa
(b) Valence transition	? $P_{tr} > 200$ GPa, $\rho_0 \sim 7.34$ Mg m ⁻³
Observed behaviour:	– $\Delta V/V \sim 4$ per cent, $P_{tr} \sim 70-80$ GPa, $K_0 \sim 200$ GPa

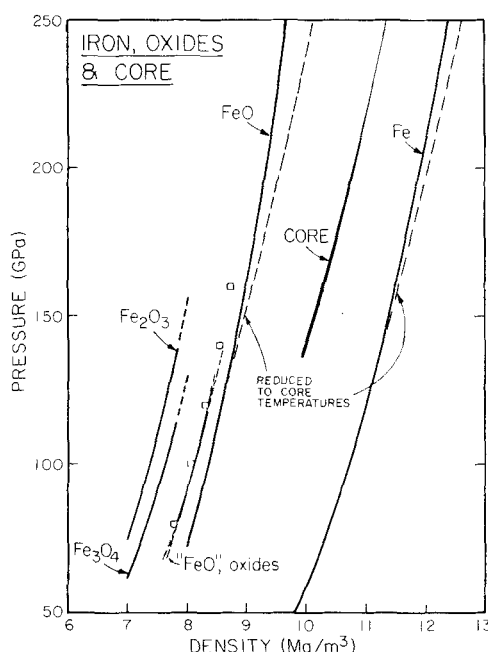


Figure 8. Shock-wave data for FeO (present results), Fe (McQueen *et al.* 1970), Fe_2O_3 and Fe_3O_4 (McQueen & Marsh, quoted in Birch 1966; not corrected for porosity) (heavy curves) compared with the seismologically determined compression curve of the core (Dziewonski, Hales & Lapwood 1975; Anderson & Hart 1976). The Fe and FeO data, corrected to core temperatures, are shown as thin dashed curves. Hugoniot of mixtures of oxides and Fe corresponding to FeO are given as thin curves: $1/3 (\text{Fe} + \text{Fe}_2\text{O}_3)$, $1/4 (\text{Fe} + \text{Fe}_3\text{O}_4)$ and $(\text{Fe}_3\text{O}_4 - \text{Fe}_2\text{O}_3)$, are plotted but overlap; open squares are from Al'tshuler & Sharipdzhanov (1971). Hugoniots for only the high-pressure phase are shown, and the wüstite data are corrected for initial porosity and non-stoichiometry (see text).

about 3 per cent), based on the shock-wave data of McQueen & Marsh (quoted in Birch 1966) and McQueen *et al.* (1970). Such assemblages would result in densities virtually identical with those of the B1 (low pressure) phase of FeO.

We point out that such comparisons can only be quantitatively made after correcting for the effects of non-stoichiometry (as well as initial porosity and Fe contamination) in the wüstite samples. This produces uncertainties due to the unknown effect of non-stoichiometry on molar volume at high pressures: we have assumed that the ratio of the molar volume for the non-stoichiometric and endmember wüstite is the same at high pressures as at zero pressure. Nevertheless, the resulting uncertainties are relatively small, and our conclusions hold (qualitatively) even when all data are reduced to a non-stoichiometry $x = 0.94$ (such a comparison is conservative since it implicitly sets the volume of vacancies equal to zero). We also note that when porosity effects are accounted for in the Hugoniot data for Fe_3O_4 and (especially) Fe_2O_3 , the Hugoniots derived for 'FeO' from mixtures of the other oxides and Fe are essentially identical (Fig. 8; $\rho\gamma = \text{constant}$, as given e.g. in Davies & Gaffney 1973).

Pressure-induced electronic transitions must be considered more speculative candidates for explaining the phase transformation in FeO since few such transitions are known among oxides. Also, there are difficulties in understanding the electronic structure of FeO (e.g. Adler 1968, 1975; Falicov & Koiller 1975), and only crude predictions can be made, as is illustrated by the example of a spin-pairing transition. According to most estimates (Fyfe

1960; Burns 1970; Gaffney & Anderson 1973; Strens 1976; Ohnishi 1978) such a transition would involve a large volume change (about 20 per cent) occurring between 25 and 55 GPa, and involving a significant increase in bulk modulus (Ohnishi & Mizutani 1978). This is inconsistent with the present data, and a spin transition could be ruled out except that Tossell (1976) has argued that it might involve only a 5 per cent volume decrease in FeO based on the work of Clack & Smith (1974) on fluorine analogues. This, along with Tossell's predicted transition pressure of 60–70 GPa, is consistent with the present data.

The possibility of a valence transition in FeO can similarly not be ruled out, although it would require the gap between 3d and 4s bands to decrease by about 2.4 eV (or more) as a compression $V/V_0 \sim 0.77$ is achieved (*cf.* Bowen, Adler & Anker 1975). This would require a significantly (~ 50 per cent) larger decrease in the band-gap upon compression than is found in EuO (Jayaraman *et al.* 1974), which only has a 1.1 eV gap at zero pressure. The density change at such a transition could be large but need not be, as is the case for EuO (~ 4 per cent: Jayaraman 1972). However, the zero-pressure density of metallic FeO of 7.34 Mg m^{-3} as calculated by Ringwood (1978) would, if correct, completely rule out metallization as the cause of the FeO transition observed in this study. Ross (1972) has argued for the validity of the Herzfeld theory of metallization which would predict an electronic collapse in FeO only at a density greater than 10.1 Mg m^{-3} , corresponding to a pressure well above 200–250 GPa. This also suggests that the present transition in FeO is not due to metallization, although it is worth noting that the density required for the electronic collapse in EuO is itself overestimated by the Herzfeld theory. Therefore, the possibility of either a spin-pairing transition or a valence transition in FeO can not be critically tested.

On the other hand, there is close agreement between the observed transition in FeO and the behaviour predicted for a B1/B2 transition, as shown in Figs 2, 6 and 7. Hence, the preferred interpretation is that FeO, like CaO, undergoes a B1/B2 transition, although the possibility of an electronic transition cannot be ruled out. The correlation in Fig. 7 is unexpectedly good, particularly since the relatively low ratio of shear to bulk moduli in FeO suggest that the B1 structure is somewhat less stable in this than in the other oxides (Jackson *et al.* 1978); the slight deviation of FeO from the trend is therefore not surprising. Although crystal-field stabilization has been invoked to explain the high-pressure phase equilibria among iron-bearing minerals (e.g. Syono, Tokonami & Matsui 1971; Burns 1976; Yagi, Mao & Bell 1978), such an effect would tend to increase the relative stability of FeO in the B1 structure, contrary to what is shown in Fig. 7.

The release adiabats determined for FeO and CaO in both their low- and high-pressure phases (Figs 2 and 3) are of interest in that they are generally internally consistent, with slopes less than the slope of the Hugoniot. This is not the case for many silicates which typically exhibit anomalous (steep) release paths from their Hugoniot states, suggesting the presence of a mixed-phase region or of non-equilibrium effects (Ahrens *et al.* 1969b; Grady, Murri & Fowles *et al.* 1974; Grady, Murri & DeCarli 1975; Jeanloz & Ahrens 1977, 1978). Entropy production due to viscous dissipation can not account for such anomalous release adiabats (Jeanloz & Ahrens 1979). The present results for simple oxides lend further confidence to the previous measurements of release adiabats, despite their often anomalous nature (see also Grady 1977). Other than the release from 161 GPa (LGG 043), which may be anomalous, the release adiabats from the Hugoniot states of CaO are shallower than would be expected for the isentropes of a solid. Although vaporization upon decompression could explain this observation, the calculated Hugoniot temperatures are lower than the melting temperature, and other effects may be involved (Lyzenga & Ahrens 1977). By contrast, the FeO release adiabats are quite similar to isentropes expected for solids. Also,

the release paths in the mixed-phase region (e.g. 84 GPa for CaO) are as expected for a momentarily 'frozen-in' transition (Ahrens *et al.* 1969b; Grady *et al.* 1974, 1975).

The Hugoniot data for CaO at 134 and 149 GPa (LGG 024 and 033 in Table 2, not shown in Fig. 3) have not been considered in the foregoing discussion. These data are anomalous, both in their extremely high densities and in their steep release adiabats. A misreading of the raw data would tend to result in anomalously shallow release paths for an erroneously high Hugoniot density, contrary to observation, and the errors associated with these data appear to be too small to account for the discrepancy. In fact, all of the data at high pressures in Fig. 3 appear to contain more scatter than is usual (e.g. Jeanloz & Ahrens 1978), and it is possible that these anomalies reflect an incipient instability in CaO. As with FeO, an electronic collapse is expected in CaO at pressures (or densities) above those achieved in this study. However, the relatively high Hugoniot temperatures which are reached above 120 GPa might help to promote such a transition (or other instability). Speculation aside, the two high density data are considered to be anomalous, and are not further discussed.

Discussion

Recently, the idea has been revived that oxygen may be an important constituent of the Earth's core (Ringwood 1978; *cf.* Jacobs 1975). Thus, one of the reasons for interest in the properties of FeO at high pressures has been in order to test its viability as a component in the core. The comparison between iron, FeO and the outer core is presented in Fig. 8, in which the shock-wave data have been reduced to core temperatures according to the analysis given above and that in Jeanloz (1979). Stacey's (1977) geotherm for the core has been used, however, the results do not depend critically on the assumed temperatures: 1500 K affects the densities by about 1 per cent, the estimated accuracy of the reduced Hugoniot data.

With the discovery of the new high-pressure phase of FeO, somewhat more oxygen can be allowed in the core, from the seismological bounds, than is implied by previous data. As is evident from Fig. 8, both the density and the compressibility (not well constrained) of an Fe–FeO mixture can reproduce the properties of the core (ideal mixing assumed): about 45 wt per cent FeO (10 wt per cent O) is required in combination with iron. This corresponds to approximately 28 atomic per cent O, or nearly a composition of Fe₂O, comprising the liquid outer core, and hence supports Ringwood's (1978) hypothesis. Although Dubrovskiy & Pan'kov (1972) had also proposed that iron oxide is present in the core, the new shock-wave data preclude their inferred composition of 100 per cent FeO. The results of this study can not be used to critically evaluate the Fe₂O hypothesis of Bullen (1973; Strens 1976), since that hypothesis is predicated on an assumed electronic transition in iron oxide, but the present data are not exactly consistent with Fe₂O comprising the outer core (by about 2.5 per cent in density).

In order to evaluate these latter hypotheses, it is crucial to resolve whether the 70 GPa transition in FeO involves an electronic transition or not. The shock-wave data allow considerable amounts of oxygen in the core on physical grounds (density, bulk modulus), however, the geochemical considerations (nature of bonding in the Fe–FeO system, whole-earth composition) can not be addressed. If oxygen occurs in the core, immiscible liquids may tend to form, as happens at zero pressure, unless FeO becomes semi-metallic (Ringwood 1978). A two-phase melt would, in this case, be highly unstable due to the large density differences between the two liquids (Fig. 8). Hence adequately vigorous stirring in the core would be required in order to prevent unmixing, unless the endmember components become more compatible at high pressures than they are at low pressures (see also Wendlandt &

Huebner 1979). Although a hypothesized electronic transition in FeO is compatible with the present data, none is required and a structural transition is quite adequate for explaining the shock-wave measurements.

An important consequence of allowing oxygen in the core is that this increases the estimated minimum temperature of the outer core, probably to about 3500 K, based on the high-pressure experiments of Usselman (1975a, b; see Jeanloz & Richter 1979, Ringwood 1978). The upper bound for temperature is still determined by the melting point of iron, which presumably can not be exceeded at the inner core/outer core boundary.

The new data for CaO and FeO can also be applied to models of the Earth's lower mantle. For example, one of the main results discussed by Jeanloz *et al.* (1979) is that CaO, as a consequence of its phase transition, has essentially the same density as the mantle at pressures above 60–70 GPa (Fig. 3). Therefore, CaO is an 'invisible' component of the lower mantle in that virtually any amount can be accommodated in accordance with seismological observations. An enrichment of CaO within the lower mantle would be compatible with an enrichment in refractory components, as suggested by inhomogeneous accretion theories.

Similarly, SiO₂ is essentially an invisible component of the lower mantle according to the available shock-wave data (e.g. Davies 1972). Although SiO₂ may have a density slightly lower than that of the mantle at high pressures (and mantle temperatures), there is significant uncertainty in the reduction of the Hugoniot data (e.g. McQueen, Fritz & Marsh 1963, 1964; Ahrens, Anderson & Ringwood 1969a; Davies 1974); the difference in densities is within about 1 per cent and hence probably not resolvable. Consequently, in terms of the major element oxides, only the relative proportions of MgO, Al₂O₃ and FeO in the lower portions of the mantle can be constrained with any assurance. At pressures less than 60–70 GPa (depths less than about 1550 km), CaO would also be considerably less dense than the mantle, unless its B2 structure is stabilized by solid solution or unless it can enter another high density phase (e.g. Liu & Ringwood 1975).

The new data for FeO do not significantly alter previous conclusions about the relative proportions of Fe in the mantle (Ringwood 1975). A value of Mg/(Mg + Fe) \sim 0.88 (\pm 0.02) satisfies mantle properties for essentially any combination of MgO, FeO and SiO₂, whereas slightly lower values are required for more than about 3–4 mol per cent Al₂O₃. On the other hand, it is possible that phases with densities slightly higher than the component oxides occur within the lower mantle, thus tending to increase this Mg-value for the total assemblage.

Of greater interest, however, is considering FeO as a candidate phase (rather than component oxide) of the lower mantle. Upper mantle olivine transforms to a perovskite + magnesiowüstite assemblage at high pressures, with iron being enriched in the oxide; these are considered likely to be the most important phases of the lower mantle (Liu 1976, 1977, 1978; Yagi *et al.* 1978; Mao, Yagi & Bell 1979). Therefore, it is of interest to extrapolate the present results across the MgO–FeO solid solution series, to plausible mantle compositions.

MgO might be expected to transform at high pressure to the B2 phase, with about a 2 per cent density increase (Fig. 6). However, shock-wave data (Carter *et al.* 1971) indicate no evidence of a transition in MgO to about 120 GPa, and this has been confirmed to 95 GPa in diamond-cell experiments (Mao & Bell 1979). But even if MgO transforms at a pressure in excess of 150 GPa, its B2 structure could still be of significance for the mantle. Interpreting the high-pressure phase of FeO as a B2 structure, a phase diagram can be constructed for (Mg, Fe)O based on the new Hugoniot data, the systematics of Fig. 6, and an assumed transition pressure for MgO. The result is Fig. 9, in which MgO is shown transforming at

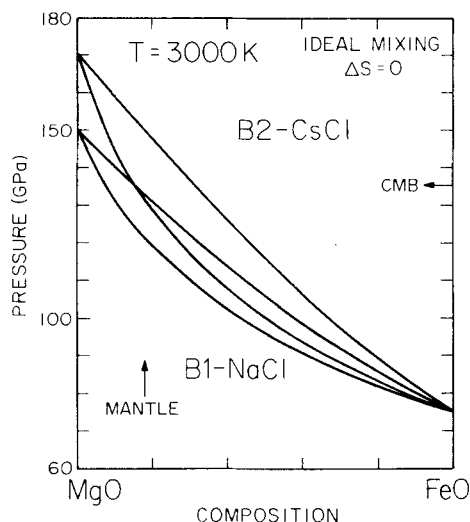


Figure 9. Calculated phase diagram for magnesiowüstite based on the present data for FeO. The pressure at the core–mantle boundary (CMB) is indicated, as is the range of plausible compositions of (Mg, Fe)O in the mantle: arrow is derived from Yagi *et al.* (1978). Ideal mixing and a zero Clapeyron slope are assumed. Two possible transition pressures for MgO are used as examples, and a temperature of 3000 K is assumed in the calculation.

150 or 170 GPa, as two examples. The plausible range of composition for (Mg, Fe)O in the mantle is indicated, as is the appropriate composition of magnesiowüstite in equilibrium with perovskite in a pyrolite-like mantle (Yagi *et al.* 1978). Thus, because of the relatively low transition pressure which has been found for FeO, a B1/B2 transition in magnesiowüstite may be of significance in the lower mantle, particularly in the D'' layer at its base.

Jeanloz & Richter (1979) recently discussed several possible explanations for the nature of the D'' region which is characterized by anomalous gradients in seismic velocities, scattering of seismic waves and possible heterogeneities (see Cleary 1974, review and references therein; also Julian & Sengupta 1973; Sacks & Beach 1974; Haddon & Cleary 1974; Kanasewitch & Gutowski 1975; Wright & Lyons 1975; Dornboos 1976; Chang & Cleary 1978). Although both compositional and thermal heterogeneities have been invoked to explain the properties of the D'' layer, the present data suggest that a third alternative, phase transition, could strongly accentuate slight variations in the temperature field near the base of the mantle, assuming a non-zero Clapeyron slope; the transition shown in Fig. 9 involves a density increase $\delta\rho \sim 5\text{--}8$ per cent in (Mg, Fe)O. A comparable density contrast requires temperature variations of 5000–10 000 K, which are highly unlikely, or compositional variations corresponding to about 10 mol per cent MgO (ideal mixing assumed throughout).

The phase assemblage near the base of the mantle is unknown, but for an olivine-rich composition perovskite might be expected as the dominant phase with up to 30 vol. per cent magnesiowüstite (~ 15 vol. per cent for a perovskite-bearing pyrolite assemblage; see Ringwood 1975; Mao *et al.* 1979). From velocity–density systematics (e.g. Birch 1961), this immediately suggests local velocity variations of 2–4 per cent in the D'' region which could readily cause scattering. Alternatively, noting that neither bulk nor shear moduli change very much upon transforming from B1 to B2 structures (Table 3; Davies 1976; Jeanloz *et al.* 1979; Cohen & Gordon 1975), the velocity is expected to decrease by about 1 per cent (for pyrolite composition) due to transformation in (Mg, Fe)O near the base of the mantle.

This could contribute to the anomalous change in velocity gradient which is observed, and the need for compositional heterogeneity in the D'' region may be precluded.

Conclusions

New shock-wave data have been presented for CaO and FeO to about 175 and 230 GPa, respectively. In both cases, a phase transformation is found at approximately 70 (± 10) GPa; it is known to be of B1/B2 type in CaO. Several candidates for the high pressure phase of FeO are allowed, but the most plausible alternative considered here appears to involve a B1/B2 structural transition.

The shock-wave data for the B1 phases of FeO and CaO are in excellent agreement with several ultrasonic and static-compression measurements on these compounds, as well as with Modified Electron Gas calculations for CaO (Cohen & Gordon 1976). Combining the available data allows a value $K'_0 \sim 3.2$ to be determined for FeO. Similarly, the properties of the high-pressure phases of CaO and FeO have been determined from a reduction of the shock-wave data (Table 3). In both cases, these properties are consistent with expectations for B2 structures based on systematics.

The main application of the FeO data is towards evaluating the possible oxygen content of the core. The new data allow a considerable amount of oxygen to be present in the core, as has recently been suggested from geochemical considerations (Ringwood 1978). However, only the physical constraints on this hypothesis can be addressed here, and establishing the nature of the transition in FeO may provide important geochemical constraints. About 28 atomic per cent substitution of oxygen in the core (the remainder being Fe) is consistent with the shock-wave data.

CaO is found to have densities essentially equivalent to those of the mantle at pressures in excess of 70 GPa. Hence it, along with SiO₂, is an invisible oxide component of the lower mantle in that there are no constraints on the amounts of these oxides which may be present. In terms of a model, mixed-oxide assemblage for the lower mantle only the relative proportions of MgO and Al₂O₃ versus FeO can be determined from density and bulk modulus data. More realistic candidate phase assemblages (e.g. perovskite-bearing) have similar properties, but probably require slightly less iron-enrichment to achieve mantle densities than the simple oxides. Nevertheless, the data for oxides allow a considerably different composition in the lower mantle than in the upper mantle. For example, an enrichment of refractory components in the lower mantle, as is suggested by inhomogeneous accretion theories (Turekian & Clark 1969), is consistent with its measured properties.

On the other hand, an application of the present data to the perovskite and oxide assemblages which is presumed to be abundant in the lower mantle, suggests that a phase transition in magnesiowüstite may be of significance within the mantle. In particular, such a transition may occur within the D'' region, suggesting the presence of only a simple thermal boundary layer at the base of the mantle and hence the possibility of another boundary layer elsewhere within the lower mantle. The most plausible cause of such a boundary layer within the mantle, and its requisite barrier to convection, is a major chemical discontinuity. The results of this study are compatible with, and perhaps suggestive of, the Earth's mantle consisting of more than one chemical and dynamic system.

Acknowledgments

We thank E. K. Graham (Pennsylvania State University), M. M. Abraham and Y. Chen (Oak Ridge National Laboratory), and R. A. Bartels (Trinity University) for providing the samples

used in this study. We have benefited from discussions with I. Jackson, M. S. T. Bukowski, E. K. Graham, J. A. Tossell, A. E. Ringwood and L. M. Falicov, as well as from the comments and help of H. K. Mao and J. W. Dewey. We thank R. Smith, E. Gelle, J. Long and H. Richeson for their assistance with the experiments. Work supported by NSF grants EAR 75-15006A01 and EAR 77-23156. Contribution number 3302, Division of Geological and Planetary Sciences, California Institute of Technology, Pasadena, California 91125.

References

- Abraham, M., Butler, C. T. & Chen, Y., 1971. Growth of high-purity and doped alkaline earth oxides: I. MgO and CaO, *J. chem. Phys.*, **55**, 3752–3756.
- Adler, D., 1968. Mechanisms for metal-nonmetal transitions in transition-metal oxides and sulfides, *Rev. mod. Phys.*, **40**, 714–736.
- Adler, D., 1975. Fundamental problems in the electronic structure of transition-metal oxides, *J. Solid State Chem.*, **12**, 332–340.
- Ahrens, T. J., Anderson, D. L. & Ringwood, A. E., 1969a. Equations of state and crystal structures of high-pressure phases of shocked silicates and oxides, *Rev. Geophys.*, **7**, 667–707.
- Ahrens, T. J., Petersen, C. F. & Rosenberg, J. T., 1969b. Shock compression of feldspars, *J. geophys. Res.*, **74**, 2727–2746.
- Ahrens, T. J., Jackson, I. & Jeanloz, R., 1977. Shock compression and adiabatic release of a titaniferous mare basalt, *Proc. 8th Lunar Sci. Conf.*, 3437–3455.
- Akimoto, S., 1972. The system MgO–FeO–SiO₂ at high pressures and temperatures – phase equilibria and elastic properties, *Tectonophysics*, **13**, 161–187.
- Al'tshuler, L. V. & Sharipdzhanov, I. I., 1971. Additive equations of state of silicates at high pressures, *Izv. Acad. Sci. USSR, Earth Phys.*, no. 3, 167–177.
- Anderson, D. L. & Hart, R. S., 1976. An earth model based on free oscillations and body waves, *J. geophys. Res.*, **81**, 1461–1475.
- Benard, J., 1954. Sur les parametres limites de la phase FeO, *Acta crystallogr.*, **7**, 214.
- Berman, H., 1939. A torsion microbalance for the determination of specific gravities of minerals, *Am. Miner.*, **24**, 434–440.
- Birch, F., 1952. Elasticity and constitution of the earth's interior, *J. geophys. Res.*, **57**, 227–286.
- Birch, F., 1961. The velocity of compressional waves in rocks to 10 kilobars, part 2, *J. geophys. Res.*, **66**, 2199–2224.
- Birch, F., 1966. Compressibility; elastic constants, in *Handbook of Physical Constants*, ed. Clark, S. P., *Geol. Soc. Am. Mem.*, **97**, 97–123.
- Bowen, H. K., Adler, D. & Anker, B. H., 1975. Electrical and optical properties of FeO, *J. Solid State Chem.*, **12**, 355–359.
- Briggs, A., 1977. Direct evidence for a brucite precipitate in a melt-grown MgO crystal, *J. Mater. Sci.*, **12**, 637–640.
- Bullen, K. E., 1973. Cores of the terrestrial planets, *Nature*, **243**, 68–70.
- Burns, R. G., 1970. *Mineralogical Applications of Crystal Field Theory*, Cambridge University Press, Cambridge, 244 pp.
- Burns, R. G., 1976. Partitioning of transition metals in mineral structures of the mantle, in *The Physics and Chemistry of Minerals and Rocks*, pp. 555–572, J. Wiley & Sons, New York.
- Carter, W. J. & Marsh, S. P., 1979. Hugoniot equations of state of polymers, unpublished report LA-UR-77-2062, Los Alamos Scientific Laboratory, New Mexico.
- Carter, W. J., Marsh, S. P., Fritz, J. N. & McQueen, R. G., 1971. The equation of state of selected materials for high-pressure reference, in *Accurate Characterization of the High-Pressure Environment*, ed. Lloyd, E. C., *Natn. Bur. Stand. U.S. Pub.* 326, pp. 147–158.
- Chang, A. C. & Cleary, J. R., 1978. Precursors to PKKP, *Bull. seism. Soc. Am.*, **68**, 1059–1079.
- Chang, Z. P. & Graham, E. K., 1977. Elastic properties of oxides in the NaCl-structure, *J. Phys. Chem. Solids*, **38**, 1355–1362.
- Chen, H., Knapp, G. S. & Chen, W. K., 1978. Extended X-ray absorption fine-structure (EXAFS) study of point defects in iron-oxides, *Ceram. Bull.*, **57**, 314.
- Clack, D. W. & Smith, W., 1974. Molecular orbital calculations on transition metal complexes, Part VIII, *J. chem. Soc., Dalton*, 2015–2020.
- Clark, S. F., Turekian, K. K. & Grossman, L., 1972. Chemical models of the Earth, in *The Nature of the Solid Earth*, pp. 3–18, ed. Robertson, E. C., McGraw-Hill, New York.

- Cleary, J. R., 1974. The D'' region, *Phys. Earth planet. Interiors*, 9, 13–27.
- Clendenen, R. L. & Drickamer, H. G., 1966. Lattice parameters of nine oxides and sulfides as a function of pressure, *J. chem. Phys.*, 44, 4223–4228.
- Cohen, A. J. & Gordon, R. G., 1975. Theory of the lattice energy, equilibrium structure, elastic constants and pressure-induced phase transitions in alkali-halide crystals, *Phys. Rev.*, 312, 3228–3241.
- Cohen, A. J. & Gordon, R. G., 1976. Modified electron-gas study of the stability, elastic properties, and high-pressure behavior of MgO and CaO crystals, *Phys. Rev.*, B14, 4593–4605.
- Davies, G. F., 1972. Equations of state and phase equilibria of stishovite and a coesitelike phase from shock-wave and other data, *J. geophys. Res.*, 77, 4920–4933.
- Davies, G. F., 1974. Limits on the constitution of the lower mantle, *Geophys. J. R. astr. Soc.*, 38, 479–503.
- Davies, G. F., 1976. The estimation of elastic properties from analogue compounds, *Geophys. J. R. astr. Soc.*, 44, 625–647.
- Davies, G. F. & Gaffney, E. S., 1973. Identification of high-pressure phases of rocks and minerals from Hugoniot data, *Geophys. J. R. astr. Soc.*, 33, 165–183.
- Demarest, H. H., Cassell, C. R. & Jamieson, J. C., 1978. The high pressure transitions in KF and RbF, *J. Phys. Chem. Solids*, 39, 1211–1215.
- Doornbos, D. J., 1976. Characteristics of lower mantle inhomogeneities from scattered waves, *Geophys. J. R. astr. Soc.*, 44, 447–470.
- Dragoo, A. L. & Spain, I. L., 1977. The elastic moduli and their pressure and temperature derivatives for calcium oxide, *J. Phys. Chem. Solids*, 38, 705–710.
- Draper, N. & Smith, H., 1966. *Applied Regression Analysis*, J. Wiley & Sons, New York, 407 pp.
- Dubrovskiy, V. A. & Pan'kov, V. L., 1972. On the composition of the earth's core, *Izv. Acad. Sci. USSR Earth Phys.*, no. 7, 452–455.
- Duvall, G. E. & Graham, R. A., 1977. Phase transitions under shock-wave loading, *Rev. mod. Phys.*, 49, 523–579.
- Dziewonski, A. M., Hales, A. L. & Lapwood, E. R., 1975. Parametrically simple earth models consistent with geophysical data, *Phys. Earth planet. Interiors*, 10, 12–48.
- Falicov, L. M. & Koiller, B., 1975. Low temperature conductivity of transition-metal oxides, *J. Solid State Chem.*, 12, 349–354.
- Freund, F. & Demortier, G., 1978. Carbon content of high-purity alkaline earth oxide single crystals grown by arc fusion, *J. Am. ceram. Soc.*, 61, 429–439.
- Freund, F., Debras, G. & Demortier, G., 1977. Carbon content of magnesium oxide single crystals grown by the arc fusion method, *J. Cryst. Growth*, 38, 277–280.
- Fritz, J. N., Marsh, S. P., Carter, W. J. & McQueen, R. G., 1971. The Hugoniot equation of state of sodium chloride in the sodium chloride structure, in *Accurate Characterization of the High-Pressure Environment*, ed. Lloyd, E. C., *Natn. Bur. Stand. US Spec. Pub.* 326, pp. 201–208.
- Fyfe, W. S., 1960. The possibility of d-electron coupling in olivine at high pressures, *Geochim. Cosmochim. Acta*, 19, 141–143.
- Gaffney, E. S. & Anderson, D. L., 1973. Effect of low-spin Fe²⁺ on the composition of the lower mantle, *J. geophys. Res.*, 78, 7005–7014.
- Grady, D. E., 1977. Processes occurring in shock-wave compression of rocks and minerals, in *High-Pressure Research*, pp. 389–438, eds Manghnani, M. H. & Akimoto, S., Academic Press, New York.
- Grady, D. E., Murri, W. J. & DeCarli, P. S., 1975. Hugoniot sound velocities and phase transformations in two silicates, *J. geophys. Res.*, 80, 4857–4861.
- Grady, D. E., Murri, W. J. & Fowles, G. R., 1974. Quartz to stishovite: wave propagation in the mixed phase region, *J. geophys. Res.*, 79, 332–338.
- Graham, E. R. & Bonczar, L. J., 1978. Elasticity of the magnesiowüstite solid solution, *EOS Trans. Am. geophys. Un.*, 59, 373.
- Haddon, R. A. W. & Cleary, J. R., 1974. Evidence for scattering of seismic PKP waves near the mantle–core boundary, *Phys. Earth planet. Interiors*, 8, 211–234.
- Hayakawa, M., Cohen, J. B. & Reed, R. B., 1972. Measurement of the lattice parameter of wüstite of high temperatures, *J. Am. ceram. Soc.*, 55, 160–164.
- Hentschel, B., 1970. Stoichiometric FeO as a metastable intermediate of the decomposition of wüstite at 255°C, *Z. Naturforsch.*, 25a, 1996–1997.
- Jackson, I. & Ahrens, T. J., 1979. Shock-wave compression of single-crystal forsterite, *J. geophys. Res.*, 84, 3039–3048.

- Jackson, I., Liebermann, R. C. & Ringwood, A. E., 1978. The elastic properties of $(\text{Mg}_x\text{Fe}_{1-x})\text{O}$ solid solutions, *Phys. Chem. Miner.*, **3**, 11–31.
- Jacobs, J. A., 1975. *The Earth's Core*, pp. 253, Academic Press, New York.
- Jayaraman, A., 1972. Pressure-induced electronic collapse and semiconductor-to-metal transition in EuO , *Phys. Rev. Lett.*, **29**, 1674–1676.
- Jayaraman, A., Singh, A. K., Chatterjee, A. & Devi, S. U., 1974. Pressure–volume relationship and pressure-induced electronic and structural transformations in Eu and Yb monochalcogenides, *Phys. Rev.*, **89**, 2513–2520.
- Jeanloz, R., 1979. Properties of iron at high pressures and the state of the core, *J. geophys. Res.*, **84**, 6059–6069.
- Jeanloz, R. & Ahrens, T. J., 1977. Pyroxenes and olivines: structural implications of shock-wave data for high pressure phases, in *High-Pressure Research*, pp. 439–461, eds Manghnani, M. H. & Akimoto, S., Academic Press, New York.
- Jeanloz, R. & Ahrens, T. J., 1978. The equation of state of a lunar anorthosite: 60025, *Proc. 9th Lunar Planet. Sci. Conf.*, 2789–2803.
- Jeanloz, R. & Ahrens, T. J., 1979. Release adiabat measurements on minerals: the effect of viscosity, *J. geophys. Res.*, **84**, 7545–7548.
- Jeanloz, R. & Ahrens, T. J., 1980. Anorthite: Thermal equation of state to high pressures, *Geophys. J. R. astr. Soc.*, **62**, 529–549.
- Jeanloz, R., Ahrens, T. J., Mao, H. K. & Bell, P. M., 1979. B1/B2 transition in CaO from shock-wave and diamond cell experiments, *Science*, **206**, 829–830.
- Jeanloz, R. & Richter, F. M., 1979. Convection, composition and the thermal state of the lower mantle, *J. geophys. Res.*, **84**, 5497–5504.
- Johnson, Q. & Mitchell, A. C., 1972. First x-ray diffraction evidence for a phase transition during shock-wave compression, *Phys. Rev. Lett.*, **29**, 1369–1371.
- Julian, B. R. & Sengupta, M. K., 1973. Seismic travel time evidence for lateral inhomogeneity in the deep mantle, *Nature*, **242**, 443–447.
- Kanasewitch, E. R. & Gutowski, P. R., 1975. Detailed seismic analysis of a lateral mantle inhomogeneity, *Earth planet. Sci. Lett.*, **25**, 379–384.
- Katsura, T., Iwasaki, B., Kimura, S. & Akimoto, S., 1967. High-pressure synthesis of the stoichiometric compound FeO , *J. chem. Phys.*, **47**, 4559–4560.
- Kofstad, P., 1972. *Nonstoichiometry, Diffusion and Electrical Conductivity in Binary Metal Oxides*, J. Wiley & Sons, New York, 382 pp.
- Liu, L.-G., 1971. A dense modification of BaO and its crystal structure, *J. appl. Phys.*, **42**, 3702–3704.
- Liu, L.-G., 1976. Orthorhombic perovskite phases observed in olivine, pyroxene and garnet at high pressures and temperatures, *Phys. Earth planet. Interiors.*, **11**, 289–298.
- Liu, L.-G., 1977. Mineralogy and chemistry of the earth's mantle above 1000 km, *Geophys. J. R. astr. Soc.*, **48**, 53–62.
- Liu, L.-G., 1978. High pressure Ca_2SiO_4 , the silicate K_2NiF_4 -isotope with crystalchemical and geophysical implications, *Phys. Chem. Miner.*, **3**, 291–299.
- Liu, L.-G. & Bassett, W. A., 1972. Effect of pressure on the crystal structure and the lattice parameters of BaO , *J. geophys. Res.*, **77**, 4934–4937.
- Liu, L.-G. & Bassett, W. A., 1973. Changes of the crystal structure and the lattice parameter of SrO at high pressure, *J. geophys. Res.*, **78**, 8470–8473.
- Liu, L.-G. & Ringwood, A. E., 1975. Synthesis of a perovskite-type polymorph of CaSiO_3 , *Earth planet. Sci. Lett.*, **28**, 209–211.
- Lyzenga, G. & Ahrens, T. J., 1978. The relations between the shock-induced free-surface velocity and post-shock density of solids, *J. Appl. Phys.*, **49**, 201–204.
- Mao, H.-K., 1974. A discussion of the iron oxides at high pressures with implications for the chemical and thermal evolution of the Earth, *Carnegie Inst. Wash. Yearbook*, **73**, 510–518.
- Mao, H.-K. & Bell, P. M., 1977. Disproportionation equilibrium in iron-bearing systems at pressures above 100 kbar with applications to chemistry of the earth's mantle, in *Energetics of Geological Processes*, pp. 236–249, eds Saxena, S. K. & Bhattacharji, S., Springer-Verlag, New York.
- Mao, H.-K. & Bell, P. M., 1979. Equations of state of MgO and $\epsilon\text{-Fe}$ under static pressure conditions, *J. geophys. Res.*, **84**, 4533–4536.
- Mao, H.-K., Takahashi, T., Bassett, W. A., Weaver, J. S. & Akimoto, S., 1969. Effect of pressure and temperature on the molar volumes of wüstite and of three $(\text{Fe}, \text{Mg})_2\text{SiO}_4$ spinel solid solutions, *J. geophys. Res.*, **74**, 1061–1069.

- Mao, H.-K., Yagi, T. & Bell, P. M., 1979. Experimental study of the relations between (Mg, Fe)SiO₃ perovskite and coexisting phases in the system MgO–FeO–SiO₂ under conditions equivalent to those in the deep mantle (150–500 kbars, 1000–1500°C), *EOS Trans. Am. geophys. Un.*, **60**, 388 (abstract).
- McQueen, R. G., Fritz, J. N. & Marsh, S. P., 1963. On the equation of state of stishovite, *J. geophys. Res.*, **68**, 2319–2322.
- McQueen, R. G., Fritz, J. N. & Marsh, S. P., 1964. On the composition of the earth's interior, *J. geophys. Res.*, **69**, 2947–2965.
- McQueen, R. G., Marsh, S. P., Taylor, J. W., Fritz, J. N. & Carter, W. J., 1970. The equation of state of solids from shock wave studies, in *High Velocity Impact Phenomena*, pp. 294–419 and appendices, ed. Kinslow, R., Academic Press, New York.
- Mood, A. M., Graybill, F. A. & Boes, D. C., 1974. *Introduction to the Theory of Statistics*, McGraw-Hill, New York, 564 pp.
- Nakamoto, K., 1970. *Infrared Spectra of Inorganic and Coordination Compounds*, 2nd edn, J. Wiley & Sons, New York, 339 pp.
- Ohnishi, S., 1978. A theory of the pressure-induced high-spin–low-spin transition of transition-metal oxides, *Phys. Earth planet. Interiors*, **17**, 130–139.
- Ohnishi, S. & Mizutani, H., 1978. Crystal-field effect on the bulk moduli of transition-metal oxides, *J. geophys. Res.*, **83**, 1852–1856.
- Pauling, L., 1960. *The Nature of the Chemical Bond*, 3rd edn, Cornell University Press, Ithaca, New York, 644 pp.
- Perez-Albuern, E. A. & Drickamer, H. G., 1965. Effect of high pressures on the compressibilities of seven crystals having the NaCl or CsCl structure, *J. chem. Phys.*, **43**, 1381–1387.
- Pistorius, C. W. F. T., 1976. Phase relations and structures of solids at high pressures, *Prog. Solid State Chem.*, **11**, 1–151.
- Ramakrishnan, J., Hardy, R. J. & Kennedy, G. C., 1979. The Grüneisen parameter γ of KBr, RbCl, and Bi through high pressure phase transitions, *J. Phys. Chem. Solids*, **40**, 297–303.
- Rice, M. H., McQueen, R. G. & Walsh, J. M., 1958. Compressibility of solids by strong shock waves, *Solid State Phys.*, **6**, 1–63.
- Ringwood, A. E., 1975. *Composition and Petrology of the Earth's Mantle*, McGraw-Hill, New York, 618 pp.
- Ringwood, A. E., 1978. Composition of the core and implications for the origin of the earth, *Geochem. J.*, **11**, 111–136.
- Robie, R. A., Hemingway, B. S. & Fisher, J. R., 1978. Thermodynamic properties of minerals and related substances, *U.S. Geol. Survey, Bull.* **1452**, Washington D.C., pp. 456.
- Ross, M., 1972. On the Herzfeld theory of metallization. Application to rare gases, alkali halides, and diatomic molecules, *J. chem. Phys.*, **56**, 4651–4653.
- Roth, W. L., 1960. Defects in the crystal and magnetic structures of ferrous oxide, *Acta crystallogr.*, **13**, 140–149.
- Sacks, I. S. & Beach, L., 1974. Lateral heterogeneity at the base of the mantle – an indication of whole mantle convection, *Carnegie Inst. Wash. Yearbook*, **73**, 1020–1032.
- Sato, Y., Ida, Y. & Akimoto, S., 1973. Equation of state determined with the Bridgman-anvil high-pressure apparatus, *High Temp.–High Press.*, **5**, 679–688.
- Shannon, R. D., 1976. Revised effective ionic radii and systematic studies of interatomic distances in halides and chalcogenides, *Acta crystallogr.*, **A32**, 751–767.
- Son, P. R. & Bartels, R. A., 1972. CaO and SrO single crystal elastic constants and their pressure derivatives, *J. Phys. Chem. Solids*, **33**, 819–828.
- Stacey, F. D., 1977. A thermal model of the earth, *Phys. Earth planet. Interiors*, **15**, 341–348.
- Strens, R. G. J., 1976. Behaviour of iron compounds at high pressure, and the stability of Fe₂O in planetary mantles, in *The Physics and Chemistry of Minerals and Rocks*, pp. 545–554, ed. Strens, R. G. J., J. Wiley & Sons, New York.
- Syono, Y., Tokonami, M. & Matsui, Y., 1971. Crystal field effect on the olivine–spinel transformation, *Phys. Earth planet. Interiors*, **4**, 347–352.
- Tossell, J. A., 1976. Electronic structures of iron-bearing oxidic minerals at high pressure, *Am. Miner.*, **61**, 130–144.
- Touloukian, Y. S., Kirby, R. K., Taylor, R. E. & Lee, T. Y. R., 1977. *Thermal Expansion, Nonmetallic Solids*, pp. 1658, IFI/Plenum, New York.
- Turekian, K. K. & Clark, S. P., Jr, 1969. Inhomogeneous accretion model of the earth from the primitive solar nebula, *Earth planet. Sci. Lett.*, **6**, 346–348.

- Usselman, T. M., 1975a. Experimental approach to the state of the core: Part I, *Am. J. Sci.*, **275**, 278–290.
- Usselman, R. M., 1975b. Experimental approach to the state of the core: Part II, *Am. J. Sci.*, **275**, 291–303.
- Vaughan, P. W. & Drickamer, H. G., 1967. High-pressure Mössbauer studies on α -Fe₂O₃, FeTiO₃ and FeO (*sic*), *J. chem. Phys.*, **47**, 1530–1536.
- Wackerle, J., 1962. Shock-wave compression of quartz, *J. appl. Phys.*, **33**, 922–937.
- Wzlsch, J. M. & Christian, R. H., 1955. Equation of state of metals from shock wave measurements, *Phys. Rev.*, **97**, 1544–1556.
- Wells, A. F., 1975. *Structural Inorganic Chemistry*, 4th edn, Oxford University Press, New York, 1095 pp.
- Wendlandt, R. F. & Huebner, J. S., 1979. Melting relations of portions of the system Fe-S-O at high pressure and applications to the composition of the earth's core, *Lunar Planet. Sci. X*, 1329–1331.
- Wright, C. & Lyons, J. A., 1975. Seismology, $dT/d\Delta$ and deep mantle convection, *Geophys. J. R. astr. Soc.*, **40**, 115–138.
- Yagi, T., Mao, H.-K. & Bell, P. M., 1978. Effect of iron on the stability and unit-cell parameters of ferromagnesian silicate perovskite, *Carnegie Inst. Wash. Yearbook*, **77**, 837–841.